Modelling Simul. Mater. Sci. Eng. **7** (1999) 253–273. Printed in the UK PII: S0965-0393(99)01663-0

Design of experiments for constitutive model selection: application to polycrystal elastoviscoplasticity

M F Horstemeyer†, D L McDowell‡ and R D McGinty‡

† Center for Materials and Engineering Sciences, Sandia National Laboratories, Livermore, CA 94551-0969, USA
‡ The George Woodruff School of Mechanical Engineering, Georgia Institute of Technology, Atlanta, GA 30332-0405, USA

Received 2 November 1998, accepted for publication 4 February 1999

Abstract. To bridge length scales in plastic flow of polycrystalline fcc metals, the salient features of 3D polycrystalline elastoviscoplasticity at the crystal level (mesoscale) were studied to determine the relative influences on macroscale behaviour. This 3D study builds upon the 2D planar double-slip analysis performed by Horstemeyer and McDowell in which the relative influence of the constitutive-law features on macroscale properties in polycrystal plasticity were quantified for oxygen-free, high-conductivity copper. The mesoscale constitutive-law features considered include single-crystal elastic properties, slip-system-level hardening law, latent hardening, slip-system-level kinematic hardening, and intergranular constraint relation. Volume-averaged macroscale responses included the effective flow stress, plastic spin, elastic moduli, hardening behaviour, and axial extension (for the free-end torsion case). Each response was evaluated at 10% and 50% effective strain levels under rectilinear shear straining. In the existing literature, only one type of behaviour (e.g. texture or stress–strain response) is typically considered when assessing these various elements of the constitutive framework. In this paper, we develop a more comprehensive understanding of the relative importance of constitutive-law features as deformation proceeds. This study suggests that the design of experiments methodology is a valuable tool to assist in selecting relevant features for polycrystalline simulations and for development of macroscale unified-creep-plasticity models. In general, the results indicated that the intergranular constraint and kinematic hardening were more influential overall than the type of constitutive model used, whether isotropic or anisotropic elasticity was used, and whether or not latent hardening was used. Finally, 3D results were similar to the previous 2D planar double-slip study of Horstemeyer and McDowell, except that latent hardening had a stronger influence on the 3D macroscale responses than the 2D macroscale responses.

1. Introduction

Continuum-slip polycrystal plasticity models have become quite popular in recent years as a tool to study deformation and texture behaviour of metals during processing (cf. Dawson (1987), Kalidindi *et al* (1992)) and shear localization (cf. Peirce *et al* (1982), Rashid *et al* (1992)). The basic elements of the theory consist of (i) slip-system hardening laws to reflect intragranular work hardening, including self- and latent-hardening components (Kocks 1976, 1987) and (ii) intergranular constraint laws to govern interactions among grains. The theory is acknowledged for providing somewhat realistic prediction/correlation of texture development and stress–strain behaviour at large strains.

Different authors have developed or recommended various forms of the basic elements of polycrystal plasticity theory that address specific applications, strain levels of interest and

0965-0393/99/020253+21$19.50

so forth. To date, however, there has been no systematic application of objective principles to discern the relative influence of various elements of the 3D theory on the collective macroscale responses. Hence, studies on different strain regimes and deformation paths have led to disparate conclusions regarding the relative importance and viability of specific forms of hardening laws, constraint relations, and other elements of constitutive laws. In this paper, we present a 'design of experiments' (DOE) methodology to quantify the relative influence of different theory elements on prediction of macroscale behaviour at various strain levels for rectilinear shearing. This methodology is intended primarily to give guidance as to which attributes should receive critical attention and which are relatively insignificant in a given application. Polycrystal elastoviscoplasticity is a good example of a highly nonlinear, coupled set of constitutive laws at the scale of individual grains which produces collective description of behaviour over many grains that is not easily traced to assumptions at the primal scale.

The DOE approach was used to quantify relative differences between effects of various mesoscale features on the macroscale volume-averaged (mean) polycrystalline responses. Such a method does not evaluate the accuracy of any given model, just the relative influence of the various nonlinear model features. The DOE approach was applied to a 2D planar double-slip elastoviscoplastic formulation (Horstemeyer and McDowell 1997) but has not been used for 3D crystal plasticity. Numerical results were correlated with the experimental torsional effective stress-strain curves for oxygen-free, high-conductivity copper (OFHC Cu). Mesoscale model features (parameters in the DOE) considered included the single-crystal elastic properties, slip-system-level hardening law, latent hardening law, slip-system-level kinematic hardening, and the intergranular constraint relation. The volume-averaged macroscale responses included the effective flow stress, texture, plastic spin, elastic moduli, hardening behaviour, and axial stress (for the fixed-end torsion case). Each response was evaluated at 10% and 50% effective strain.

The DOE is a statistical analysis that employs orthogonality principles to evaluate the relative influence of mesoscale model features on the macroscale responses. This sensitivity study is the first of its type known to the authors applied to the various elements of 3D polycrystalline plasticity theory. Essentially, the DOE approach offers the capability to assess the sensitivity of the macroscale model predications to various independent features of the mesoscale constitutive relations. This methodology is not limited to polycrystalline metals, although that is the context of this article. After presenting the methodology, we consider the influence of various parameters:

(a) whether the single crystal elastic properties are isotropic or anisotropic;
(b) the type of intergranular constraint employed: Taylor (1938) or finite-element method
(c) effects of latent hardening versus Taylor hardening;
(d) the form of hardening model used: Armstrong and Frederick (1966) or Rashid and Nemat Nasser (1990);
(e) whether or not slip-system kinematic hardening is used (Horstemeyer and McDowell 1997).

The responses given by the macroscale volume-averaged quantities (effective flow stress, work-hardening rate, plastic spin, elastic moduli, and axial extension) are then discussed. Finally, some comparisons with the planar double-slip study are discussed.

2. Statistical design of experiments technique

The earliest works that relate statistical procedures to physical experiments were due to Sir Ronald Fisher (1935a, b). As a result of his work, statisticians used several analysis of variance

techniques to interpret physical experimental data (Box *et al* 1978). DOE is one such technique. Taguchi (1974, 1986, 1987) popularized the DOE method for use in the quality-engineering area. Nelder and Lee (1991) discussed the use of linear statistical models for DOE analysis. Nair and Shoemaker (1990) reviewed various applications of the DOE. Nair (1992) led a panel discussion covering the mathematical and practical applications of DOE methods. In the present DOE study, the 'experiments' are not physical but numerical in nature.

An investigator can select a number of levels for each variable or parameter and then run experiments to evaluate the parametric effect in an efficient manner. Hence, any number of levels or parameters can be placed in an orthogonal array so as to efficiently determine the parametric effects. Orthogonality refers to statistically independent or balanced parameters that make up the columns of the array. Once the number of levels and parameters are determined, an orthogonal array is set up to determine the number of experiments needed (Taguchi 1986, 1987). The terminology of orthogonal arrays $L_x(y^z)$ is as follows. 'x' denotes the number of calculations in the experiment, 'y' denotes the number of levels, and 'z' denotes the number of parameters. For example, to examine eight parameters at three levels, one would have an orthogonal array represented by $L_{18}(3^8)$ (cf. Taguchi (1986)) which would reduce the number of calculations if performed linearly in series from 6561 to 18.

For the purposes of understanding the relative influence of the various polycrystalline mesoscale model features on macroscale responses, only two levels were chosen with five independent variables. As such, the appropriate orthogonal array is the L_8 array. The L_8 represents an orthogonal array of equations represented by eight 'experiments'. The L_8 array allows up to seven independent *parameters* with two levels for each parameter. Each *level* can be characterized by an appropriate attribute. For example, the *parameter* could be the intergranular constraint, and the two *levels* might be defined by either the Taylor constraint (Taylor 1938) or use of the finite-element method. Although a full factorial set of calculations could be performed to vary each parameter in a linear fashion, a DOE reduces the set of calculations in a repeatable, cost-effective manner such that data can be easily translated into meaningful and verifiable conclusions. With this technique, relevant data can be extracted from a relatively small number of experiments (or numerical calculations). Clearly, the advantages of DOE as a screening process for parameter influence grow exponentially as the number of parameter variations increases. Table 1 shows the L_8 array of calculations performed in the present example.

Table 1. L_8 orthogonal array showing the parameters.

Calculation	Kinematic hardening	Latent hardening	Hardening model	Intergranular constraint	Elastic properties
1	Yes	1.0	AF	FEM	Anisotropic
2	Yes	1.0	AF	Taylor	Isotropic
3	Yes	1.4	RNN	FEM	Anisotropic
4	Yes	1.4	RNN	Taylor	Isotropic
5	No	1.0	RNN	FEM	Isotropic
6	No	1.0	RNN	Taylor	Anisotropic
7	No	1.4	AF	FEM	Isotropic
8	No	1.4	AF	Taylor	Anisotropic

3. Mesoscale influence parameters

In this section, we describe each parameter with its corresponding two levels. The term 'model feature' is used interchangeably with 'parameter' in this context since we have focussed on constitutive models. Before the model features are discussed, some explanation for the crystalline kinematics is in order to show that all the model features are interdependent. For example in a current configuration formulation, three main coupled ordinary differential equations need to be simultaneously solved, i.e.

$$\dot{\underline{\sigma}} = \underline{W}^{\mathrm{e}}\underline{\sigma} - \underline{\sigma}\underline{W}^{\mathrm{e}} + \underline{\underline{C}}^{*} : \left(\underline{D} - \hat{\underline{D}}^{\mathrm{p}}\right) + \underline{\underline{C}}^{*} : \left[\hat{\underline{W}}^{\mathrm{p}}\left(\underline{\underline{B}}^{*} : \underline{\sigma}\right) - \left(\underline{\underline{B}}^{*} : \underline{\sigma}\right)\hat{\underline{W}}^{\mathrm{p}}\right] \tag{1}$$

$$\underline{D} = \underline{D}^{\mathrm{e}} + \hat{\underline{D}}^{\mathrm{p}} + \left(\underline{\underline{B}}^{*} : \underline{\sigma}\right)\hat{\underline{W}}^{\mathrm{p}} - \hat{\underline{W}}^{\mathrm{p}}\left(\underline{\underline{B}}^{*} : \underline{\sigma}\right) \tag{2}$$

$$\underline{W} = \underline{W}^{\mathrm{e}} + \hat{\underline{W}}^{\mathrm{p}} + \left(\underline{\underline{B}}^{*} : \underline{\sigma}\right)\hat{\underline{D}}^{\mathrm{p}} - \hat{\underline{D}}^{\mathrm{p}}\left(\underline{\underline{B}}^{*} : \underline{\sigma}\right) \tag{3}$$

where $\underline{\sigma}$ is the Cauchy stress, $\underline{D}$ is the rate of deformation, $\underline{W}$ is the continuum spin, $\underline{D}^{\mathrm{e}}$ is the elastic rate of deformation, $\underline{W}^{\mathrm{e}}$ is the elastic spin, $\hat{\underline{D}}^{\mathrm{p}}$ is the plastic rate of deformation, $\hat{\underline{W}}^{\mathrm{p}}$ is the plastic spin, $\underline{\underline{C}}^{*}$ is the elastic moduli rotated to the current configuration, and $\underline{\underline{B}}^{*}$ is the elastic compliance rotated to the current configuration. The different terms arise when the multiplicative decomposition of the deformation gradient is divided into elastic (including rigid lattice rotation) and plastic parts, i.e. $\underline{F} = \underline{F}^{\mathrm{e}}\underline{F}^{\mathrm{p}}$.

$\underline{F}^{\mathrm{p}}$ is computed at the end of the time step by applying the Cayley–Hamilton theorem,

$$\underline{F}^{\mathrm{p}}_{t+\Delta t} = \exp\left(\underline{L}^{\mathrm{p}}\Delta t\right)\underline{F}^{\mathrm{p}}_{t} \tag{4}$$

where $\underline{F}^{\mathrm{p}}_{t}$ and $\underline{F}^{\mathrm{p}}_{t+\Delta t}$ are the plastic deformation gradients at the beginning and end of the time step, respectively. $\underline{L}^{\mathrm{p}}$ is the plastic velocity gradient in the intermediate configuration that occurs during the time step, which is determined by (Asaro 1983)

$$\underline{L}^{\mathrm{p}} = \sum_{i=1}^{N} \dot{\gamma}_i \left(\underline{s}_i \otimes \underline{m}_i\right) \tag{5}$$

where N is the number of slip systems, $\dot{\gamma}_i$ is the continuum slip or shear rate on the ith slip system, $\underline{s}_i$ is the slip direction vector, and $\underline{m}_i$ is the slip-plane normal vector.

The focus of this paper is not to identify the absolute accuracy of specific models of microstructural phenomena; many representations exist to model hardening, for example, that may be more accurate than either the Rashid–Nemat Nasser hardening rule or the Armstrong–Frederick (Armstrong and Frederick 1966) form used in this work. We focus instead on an objective methodology by which we can assess the relative influence of various elements or model features within a complex, highly nonlinear and coupled constitutive framework such as polycrystal plasticity. This is relevant to sorting out key mesostructure, macro-property relationships that should receive particular attention in building up robust, physically based models. Although humans (particularly experts!) can assimilate such relative comparisons in manual fashion to a reasonable degree, such assessments are often biassed towards pre-conceived notions of proper model components or assemblages thereof. Specifically, in the context of the hierarchical modelling ideas discussed by Olson (1997), we contend that the DOE methodology may provide quantitative indication of cause-and-effect between micro/mesostructure and performance at the macroscopic level, thereby focussing attention on the most salient elements of evolving microstructure. As Olson puts it,

> ...much of materials science is the art of discriminating the essential from the nonessential...as we unravel the complex products of empirical development to control desired properties. It is reciprocity that gives us the tools for materials design.

Olson mentions the reciprocity principle first elaborated by Cohen (1976), which states that although we typically regard properties as controlled by structure, we may also regard structure as controlled by properties in terms of our conception or idealization of that structure. This permits us to distil simplicity from complexity by focussing on specific properties or performance attributes. In this case, we are interested in discerning the appropriate tools for modelling structure–property relations, assuming that mesoscale structure evolution is represented in the phenomenological sets of grain-level constitutive laws. Orthogonal statistical DOE methods are rather well suited for this algorithm. To proceed, it is necessary to identify those macroscopic performance goals/parameters of most interest. Then, the relative importance of the microstructural model features changes as a function of the selected set of material performance indices.

We next consider examples of different mesoscale representations/models which will be used to examine relative effects on the macroscale response function of the polycrystalline aggregate. Those selected here for illustration are of a very well established, simple character and are chosen to provide a wide range of description at the mesoscale (i.e. single grain or small sets of grains).

3.1. Isotropic versus anisotropic elasticity

Elastic properties arise from the binding forces of atoms as affected by the distance between them. The elastic properties of single crystals can be highly anisotropic and can vary with the orientation of the crystal lattice.

The hyperelastic relation is specified in the intermediate, or stress-free, configuration as

$$\underline{\hat{\sigma}}\left(\underline{\hat{E}}\right) = \underline{\underline{C}} : \underline{\hat{E}} \tag{6}$$

where the elastic stiffness tensor, $\underline{\underline{C}}$, is invariant for a given crystal in the intermediate configuration (cf. Asaro (1983)). The intermediate configuration is aligned with the crystalline axes. $\underline{\hat{\sigma}}$ is the second Piola–Kirchhoff stress in the intermediate configuration, and $\underline{\hat{E}}$ is the conjugate Green elastic strain. For cubic orthotropy, the single-crystal elastic moduli are formed on axes of cubic symmetry ($\langle 100\rangle$, $\langle 010\rangle$, and $\langle 001\rangle$ axes). By defining

$$\begin{aligned} C_1 &= C_{1111} = C_{2222} = C_{3333} \\ C_2 &= C_{1122} = C_{2233} = C_{1133} \\ C_3 &= C_{1212} = C_{1313} = C_{2323} \end{aligned} \tag{7}$$

the components are formed on the cartesian axes coincident with ($\langle 100\rangle$, $\langle 010\rangle$, and $\langle 001\rangle$ axes) with all other C_{ijkl} equal to zero. The stress in the current configuration is related to the second Piola–Kirchhoff stress by

$$\underline{\sigma} = \frac{1}{J}\underline{F}^{\mathrm{e}}\,\underline{\hat{\sigma}}\,\underline{F}^{\mathrm{eT}}. \tag{8}$$

Now the Zener anisotropy factor as related to the crystal axis (not the specimen axis) is given by

$$Z = \frac{2C_3}{C_1 - C_2}. \tag{9}$$

When $Z = 1$, the elastic properties are isotropic; however, $Z > 3$ for Cu single crystals. In finite inelastic deformation, grains rotate and tend to align themselves statistically toward a pole. As each grain rotates, elasticity is considered to influence macroscale mechanical behaviour (France *et al* 1967). Lowe and Lipkin (1990) showed that anisotropic single-crystal elastic properties are necessary for determining macroscale responses under non-monotonic

loading conditions at finite strain. Cuitino and Ortiz (1992) used anisotropic single-crystal elastic properties for a strain-localization problem. Alternatively, Rashid *et al* (1992), in the spirit of Lin (1957), used isotropic single-crystal properties and showed that localization (and strain softening) does not depend on elastic anisotropy. None of these works compared isotropic and anisotropic elasticity directly.

The elastic properties in this study are used to compare the influence of single-crystal isotropic versus anisotropic elasticity. The single-crystal elastic constants used are given in table A1 in the appendix.

3.2. Intergranular constraint relation

The intergranular constraint plays a crucial role in determining accurate macroscale responses (Honneff and Mecking 1978), since each grain is assumed to possess a distinct crystallographic orientation. Hence, the intergranular constraint controls the effects of crystallographic misorientations among grains. In the DOE study we use a Taylor-type (Taylor 1938) constraint and the finite-element method as two different models. For each analysis, 198 randomly oriented grains were used. The same deformation was applied to all the grains in the Taylor analysis. For the finite-element analysis, a 2D plane strain finite-element mesh was used that allowed 3D rotations for the crystals.

We used the finite-element code ABAQUS for our analyses, in which single-crystal orientations were used in different elements of the mesh (cf. Kalidindi and Anand (1991), Kalidindi *et al* (1992), Dawson *et al* (1994)). By using finite elements, the constraints among grains will relax as deformation proceeds along the lines of a self-consistent modelling introduced earlier by Hutchinson (1970). The mesh comprised 15 rows by 30 columns of elements. Uniform uniaxial displacements were applied to the mesh. Only the responses of the central 198 elements/grains (9 rows by 22 columns) were included in the DOE study in order to minimize the influences of the boundary conditions.

To solve the polycrystalline boundary-value problem using a single-crystal analysis without finite elements, an averaging procedure is needed which employs some assumption for the intergranular constraint. A crystal-to-aggregate averaging theorem (Bishop and Hill 1951, Hill 1965, Hill and Rice 1972) was developed based on an assumption by Taylor (1938) that the deformation gradient in each grain is the same. Other types of intergranular constraints have also been assumed (cf. Eshelby (1957), Kroner (1961), Budiansky and Wu (1962), Honneff and Mecking (1978), Berveiller and Zaoui (1979), etc). The Taylor constraint produces an upper bound estimate for flow stress since it ensures compatibility but not equilibrium.

3.3. Hardening models with and without latent hardening

The viscoplastic kinetic relation used in this study is a kinematic hardening generalization of the form employed by Hutchinson (1976), i.e.

$$\dot{\gamma}_i = \dot{\gamma}_o \operatorname{sgn}(\tau_i - \alpha_i) \left| \frac{\tau_i - \alpha_i}{g_i} \right|^M \tag{10}$$

where the plastic slip rate on the ith slip system, $\dot{\gamma}_i$, is a function of a fixed reference strain rate, $\dot{\gamma}_o$, the reference shear strength, g_i, the resolved shear stress on the slip system, τ_i, the rate sensitivity exponent for the material, M, and an internal state variable representing kinematic hardening effects resulting from backstress at the slip-system level, α_i.

Two forms of the hardening law were chosen for evaluation in the DOE, the Armstrong–Frederick (Armstrong and Frederick 1966) and Rashid–Nemat Nasser model (Rashid and

Nemat Nasser 1990). The Armstrong–Frederick form contains an isotropic hardening evolution law for the internal hardening state variable, g_i, on ith slip system given by

$$\dot{g}_i = A \sum_{j=1}^{12} q_{ij} \left|\dot{\gamma}_j\right| - B g_i \sum_{j=1}^{12} \left|\dot{\gamma}_j\right| \tag{11}$$

where A and B are the hardening and recovery moduli used to fit the experimental data, and q_{ij} is the latent hardening ratio that was set to 1.0 for Taylor hardening and 1.4 for stronger latent hardening in the DOE study. The self-hardening components arise when $i = j$ and the latent hardening components arise when $i \neq j$. Note that for OFHC Cu the number of potential slip systems is 12.

The increase or decrease in flow stress on a secondary slip system due to crystallographic slip on an active slip system is referred to as latent hardening. Taylor and Elam (1923), based on experimental evidence on aluminum crystals, observed that when latent hardening equals self-hardening, an isotropic response exists. Kocks (1970) reviewed the behaviour of several materials under different loading conditions and surmised that an intersecting slip system induces higher stresses in the well-developed flow-stress regime. The latent hardening ratio, which is the ratio of hardening on the secondary system compared with the primary system, ranges from 1.0 to 1.4 for the form used by Hutchinson (1976) and Peirce *et al* (1982), sometimes called the PAN rule, where 1.0 corresponds to Taylor hardening.

Hansen and Jensen (1991) showed for tensile tests that texture and conventional latent hardening effects cannot account for all sources of anisotropy, in general. In essence, latent hardening models have focussed on dislocation–dislocation interactions, but in reality latent hardening arises from dislocation–substructure interactions as well. In the latter case, an evolving latent hardening ratio would be necessary. Although potentially important, an evolving latent hardening ratio is beyond the scope of this study. We employ the simplified PAN rule for latent hardening as

$$q_{ij} = \left[\delta_{ij} + lhr\left(1 - \delta_{ij}\right)\right] \tag{12}$$

where lhr is the latent hardening ratio, and δ_{ij} is the Kronecker delta.

Other latent hardening forms have been proposed and might be fruitful to consider in such parameter studies; for example, Weng (1987) claimed that equation (12) is suitable for monotonic loadings but does not appropriately represent the forward and reverse interactions of crystallographic slip. Furthermore, it cannot distinguish between acute and obtuse cross slips in reversed quasi-static loading conditions. Weng (1987) proposed a rate-independent, three-parameter model for latent hardening representing forest dislocation features that correlated with Phillips' (Phillips and Gray 1961, Phillips and Kasper 1973, Phillips and Das 1985) measured initial and subsequent yield surfaces under combined stress fields. Havner (1982) employed a two-parameter rule of Nakada and Keh (1966) to examine latent hardening effects, showing that the contribution of incremental slip from self-hardening equals that of the latent system. Bassani and Wu (1991) have introduced a self-hardening formulation that has captured some of the apparent latent hardening effects.

Other issues regarding latent hardening that are not included in this work include differences that have been observed from one latent system to the next. Franciosi *et al* (1980) determined in Cu and Al single crystals that slip systems in which dislocations can form sessile junctions appear to exhibit primary latent hardening. Secondary latent hardening is associated with systems for which dislocations form glissile junctions or Hirth locks with those of the active slip systems. Also not considered is the influence of the stacking-fault energy; the lower the stacking-fault energy, the higher the latent hardening. Models to date only empirically fit constants to the latent hardening equation and physical motivation is often lacking. Finally,

although the latent hardening ratio seems to be independent of temperature, alloy type, and strain rate (Kocks 1970), it does change during deformation, saturating at a strain of the order of unity. In this study, $lhr = 1.0$ and $lhr = 1.4$ as shown in table 1.

Like the Armstrong–Frederick form, the Rashid and Nemat Nasser (1990) isotropic hardening rule is given with the latent hardening ratio as

$$\dot{g}_i = \begin{cases} h_0 & 0 \leqslant \gamma \leqslant \gamma_0 \\ \displaystyle\sum_{j=1}^{12} \frac{h_0 q_{ij} \left|\gamma_j\right|}{1 + \Phi\left(\left|\gamma_j\right| - \gamma_0\right)} & \gamma_0 \leqslant \gamma \end{cases} \tag{13}$$

where h_0, Φ, and γ_0 are material constants.

3.4. Slip-system-level isotropic–kinematic hardening or isotropic hardening

The role of grain-level kinematic hardening was examined in this DOE study to assess its comparative influence on the macroscale responses. Kinematic hardening at the grain level is used to model dislocation substructure contribution to the directional dislocation resistance. Kinematic hardening at the level of the slip system has been rather widely employed to describe strengthening due to heterogeneous dislocation substructure and attendant Bauschinger effects (cf. Jordan and Walker (1992)). We employ a substructural internal variable evolution equation (Horstemeyer and McDowell 1998). From the work of Horstemeyer and McDowell (1998), calculations were performed that illustrated the effects of the single-crystal kinematic hardening on texture evolution and stress–strain behaviour. For the Armstrong–Frederick and Rashid–Nemat Nasser forms, we employ the following equation for each crystal

$$\underline{\dot{\alpha}}_i = C_{\text{rate}} \left(C_{\text{sat}} \underline{\dot{\gamma}}_i - \alpha_i \left\| \dot{\gamma}_i \right\| \right) \tag{14}$$

where C_{rate} controls the rate of evolution, and C_{sat} is the saturation level of the backstress, where these were chosen to fit the experimental data. The substructural hardening internal state variable reflects dislocation interactions within the grain (cf. Rice (1971)) and follows the postulate of Coleman and Gurtin (1967) that the rate must be governed by a differential equation in which the plastic rate of deformation appears.

We note that a saturation value for the kinematic hardening was chosen to be about 20% of the effective flow stress at 30% strain. If the saturation value occurred at a lower strain level or higher strain level, the conclusions of this DOE study might be different. However, this level of kinematic hardening is deemed physically consistent with substructure formation in pure metals and considerably less than that which might be produced in complex two-phase microstructures (cf. Kocks (1976, 1987)). For non-zero $\underline{\alpha}$, the flow rule in equation (14) is used and in the DOE represents 'yes'. When kinematic hardening is 'no' in table 1, $\underline{\alpha} = \underline{0}$.

It is well known that a certain degree of kinematic hardening (Bauschinger effect) is introduced by virtue of the orientation dependence of grains and compatibility requirements among them in polycrystal plasticity theory. However, this is a highly transient effect that occurs over small cumulative plastic strain following a strain reversal. More persistent Bauschinger effects arise from prescription of kinematic hardening at the scale of individual grains (slip systems), affecting slip-system flow rules. Reversed-loading experiments on single crystals of both precipitate-strengthened (cf. Jordan *et al* 1993) and pure metals (cf. Mughrabi 1978) exhibit kinematic hardening due to heterogeneous inelastic flow. Precipitates offer a clear source of the behaviour in the former. Dislocation substructures induce these effects in the latter. In the latter case, the backstress is induced by the collective effects of interactions with dislocation structures at higher scales.

4. Macroscale responses

Certain *macroscale* responses (attributes) were used to assess the relative importance of the *mesoscale* model features. Essentially, these responses serve as performance indices or requirements at the macroscale. One such macroscale response is the polycrystalline effective (von Mises) flow stress, which was correlated with the experimental data under free-end torsion conditions based only on the first-order response, i.e. $\sigma^{\text{eff}} = \sqrt{3}\sigma_{12}^{\text{ave}}$. Each of the eight calculations was correlated with the torsional data and remained at least within 6% of the stress level throughout the straining period. Table 2 summarizes the effective flow-stress levels at 10% and 50% strain for the eight calculations and the experimental data to illustrate the close approximations.

Table 2. Effective (von Mises) stress (MPa) from calculations and from experimental torsional data for OFHC Cu.

Calculation	10% eff. strain	50% eff. strain
1	130	241
2	128	241
3	132	251
4	128	240
5	123	235
6	123	236
7	121	241
8	121	241
Exp. result	123	240

Table A1 in the appendix summarizes the material constants that were used to determine these stress–strain responses. We note that the material constants are not unique.

Another macroscale response is the plastic spin that is related to texture. We employ aspects from the orientation distribution function (ODF), which depicts the evolution of texture as a function of effective strain. The ODF has two components: mean and spread, the mean being defined by the volume average over the polycrystalline distribution and the spread (assuming Gaussian distribution) being defined by the standard deviation of the polycrystalline distribution. Horstemeyer and McDowell (1997) showed how this procedure was used to relate the pole and distribution of texture to the mean and spread of plastic spin and the work-hardening rate. Other macroscale responses of interest were the polycrystalline elastic moduli and development of polycrystalline axial extension in free-end shear which were determined by the volume averages of the single-crystal quantities.

From the L_8 array, we may write

$$[R] = [P][A] \tag{15}$$

where $[R]$ is the response matrix, $[A]$ is the output matrix and indicates the relative influence of the crystal plasticity model feature, and $[P]$ is the parameter matrix. Each is denoted by

$$[R] = \begin{bmatrix} R_1 \\ R_2 \\ R_3 \\ R_4 \\ R_5 \\ R_6 \\ R_7 \\ R_8 \end{bmatrix} \quad [A] = \begin{bmatrix} 2A_1 \\ A_2 \\ A_3 \\ A_4 \\ A_5 \\ A_6 \\ A_7 \\ A_8 \end{bmatrix} \quad [P] = \begin{bmatrix} +1 & +1 & -1 & -1 & -1 & -1 & +1 & +1 \\ +1 & +1 & -1 & -1 & +1 & +1 & -1 & -1 \\ +1 & +1 & +1 & +1 & -1 & -1 & -1 & -1 \\ +1 & +1 & +1 & +1 & +1 & +1 & +1 & +1 \\ +1 & -1 & -1 & +1 & -1 & +1 & -1 & +1 \\ +1 & -1 & -1 & +1 & +1 & -1 & +1 & -1 \\ +1 & -1 & +1 & -1 & -1 & +1 & +1 & -1 \\ +1 & -1 & +1 & -1 & +1 & -1 & -1 & +1 \end{bmatrix} \tag{16}$$

The parameter matrix $[P]$, shown in equation (16), has an equal number of occurrences in each column. For each level within a column, each level within any other column will occur an equal number of times as well. This introduces the statistical independence or balance into the orthogonal array. If the results, $[R]$, associated with one level change to another level, then the parameter from one level to another has a strong impact on the macroscale response being considered. Because different levels occur an equal number of times, an effect on the macroscale response by the other parameters is cancelled out. Hence, the -1's and $+1$'s in matrix $[P]$ are simply used to express the effect of the two different levels.

The values for the R-matrix, for example, for torsional effective stresses are given in table 2. The mean of the results from the DOE analysis is given by A_1. A_2 is the output from the eight calculations under the parameter related to the slip-system-level kinematic hardening. A_3 reflects influence from latent hardening. A_4 depends on the type of hardening model that was used. A_5 relates to the type of intergranular constraint used. A_6 relates to the single-crystal elastic moduli that were used. DOE outputs A_7–A_8 are the outputs related to the second-order interaction of parameters. These second-order responses turned out to be negligible in the analysis. Note that A_1–A_8 do not have physical significance in an absolute sense, just statistical significance in expressing the relative influence of associated model features on the response matrix, R. Furthermore, we note that we are assuming a statistical linear dependence of terms so only two levels of each parameter were chosen. If more levels are desired, another orthogonal array would be necessary and a higher-order statistical assumption would have to be made.

The matrix of outputs, $[A]$, can be determined by inverting the parameter matrix, $[P]$. In the parameter matrix, -1 is placed where kinematic hardening is 'no' (recall table 1). The same is done when latent hardening is '1.0', when the hardening model is AF, when the intergranular constraint is FEM, and when the elastic properties are anisotropic. In contrast, $+1$ is placed in the table when the kinematic hardening is 'yes', and so on. Since the response is determined from the finite-element calculations and is hence known, the DOE outputs A_1–A_8 can be determined from equation (16). These outputs are then used to quantify the parametric effects of the model features.

4.1. Example: effective stress at 50% effective strain

For the sake of brevity, an example is presented of a macroscale response (effective flow stress) to illustrate the methodology, corresponding to 50% strain. The details of the determination of the output values for the other macroscale responses will not be discussed later in the paper, only the results. For the effective stress response at 50% strain, the kinematic output level $A_2 = 20$, the latent hardening output level $A_3 = 20$, the hardening model output level $A_4 = 2$, the intergranular constraint output level $A_5 = 10$, and the elastic properties output level $A_6 = 12$. Since these values arise relative to each other, the values were normalized to the largest value among them in order to assess the relative level of influence of each parameter. Table 3 shows the values for the outputs when examining the effective stress level. Constant A_1 is the average and is not relevant to our parametric study so is not included in the discussion.

Hence, the most influential model features at 50% effective strain, when examining the effective stress, were the kinematic hardening and latent hardening. The gradation that will be used to describe the magnitude of influence is: (a) primary: 85–100%; (b) secondary: 60–85%; (c) tertiary: 30–60%; (d) minor: 20–30%; (e) negligible: 0–20%.

Since the kinematic hardening and latent hardening have the highest statistical value, they are the primary influence on the effective stress at 50% strain. The intergranular constraint and effects of elasticity have a tertiary influence, and the effect of the hardening model is negligible.

Table 3. Output values for effective flow stress at 50% effective strain.

Parameter	Constant value	Normalized value
Kinematic hardening, A_2	20	1.00
Latent hardening, A_3	20	1.00
Hardening model, A_4	2	0.10
Intergranular constraint, A_5	10	0.50
Elastic properties, A_6	12	0.60

Figure 1 shows the relative influences for the effective stress at 10% and 50% strain. These two levels were chosen to illustrate the evolving influence as deformation proceeds from 'small' finite strains to 'moderate' finite strains.

5. Discussion of results

There are two perspectives from which to view these data in this study. One perspective views how each parameter affects the different macroscale responses. The other perspective examines how each macroscale response is affected by the parameters. We shall discuss the parameter paradigm first in figures 1–5. We shall then discuss the macroscale response paradigm in figures 6–12.

5.1. Parameter discussion

Figure 1 summarizes the normalized results from DOE study for the influence of the intergranular constraint on the macroscale responses. As one can see, the intergranular constraint was the primary influence at 10% strain on the spread of the work-hardening rate, the spread of plastic spin, elasticity, and axial extension. Because the constraint assumption relaxes or confines the diffusion of the texture as deformation proceeds, we see a strong effect

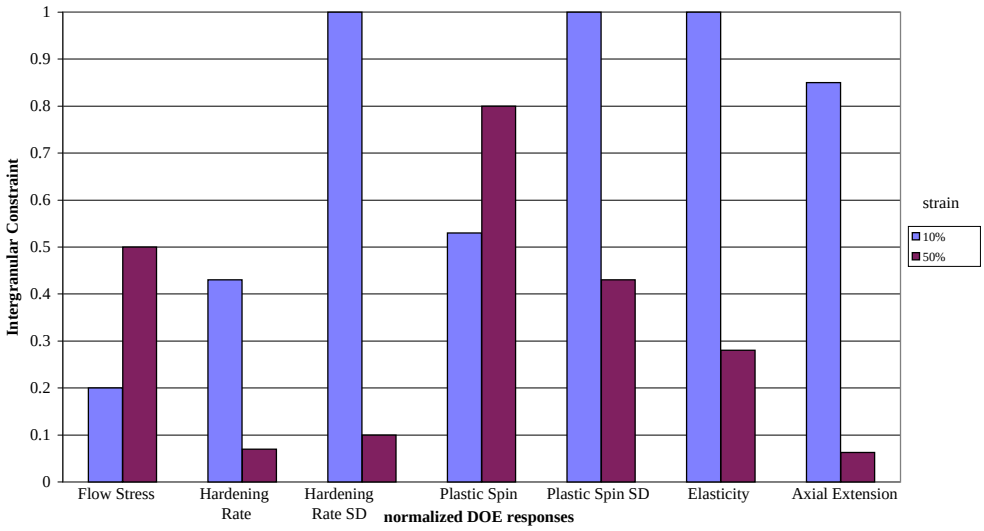

Figure 1. DOE influence of intergranular constraint on responses at 10% and 50% effective strain.

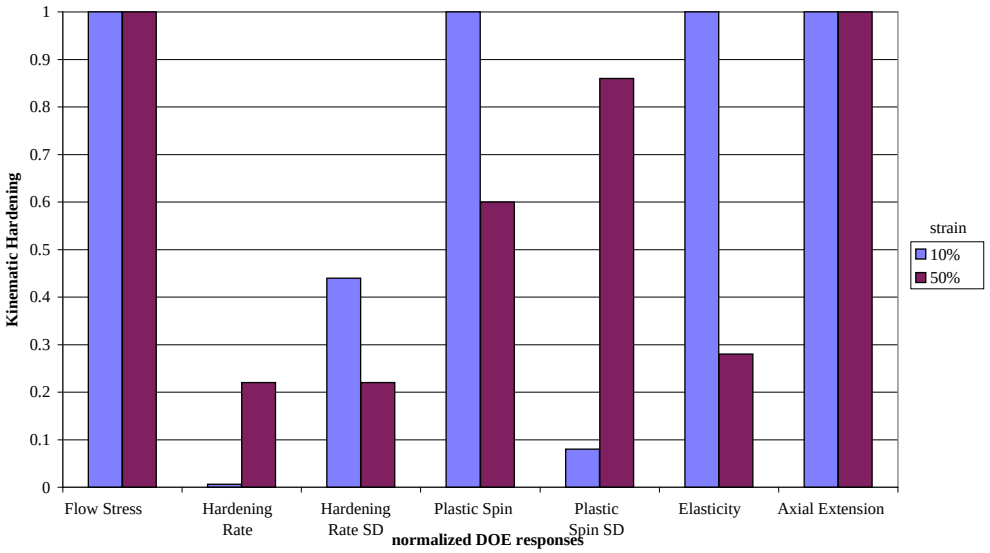

Figure 2. DOE influence of kinematic hardening on responses at 10% and 50% effective strain.

on the distribution spread of the plastic spin and work-hardening rate. These two macroscale responses are directly a function of the texture evolution. The influence of the intergranular constraint is lessened as deformation proceeds.

The kinematic hardening had the most influence over the macroscale responses, more than any other feature of the model at both levels of strain examined (10% and 50%). Figure 2 shows that primary influence over flow stress, axial extension, plastic spin, elasticity at a lower strain, and plastic spin spread at a higher strain. It had much less influence on the mean and spread of the work-hardening rate. This is interesting since the kinematic hardening saturated

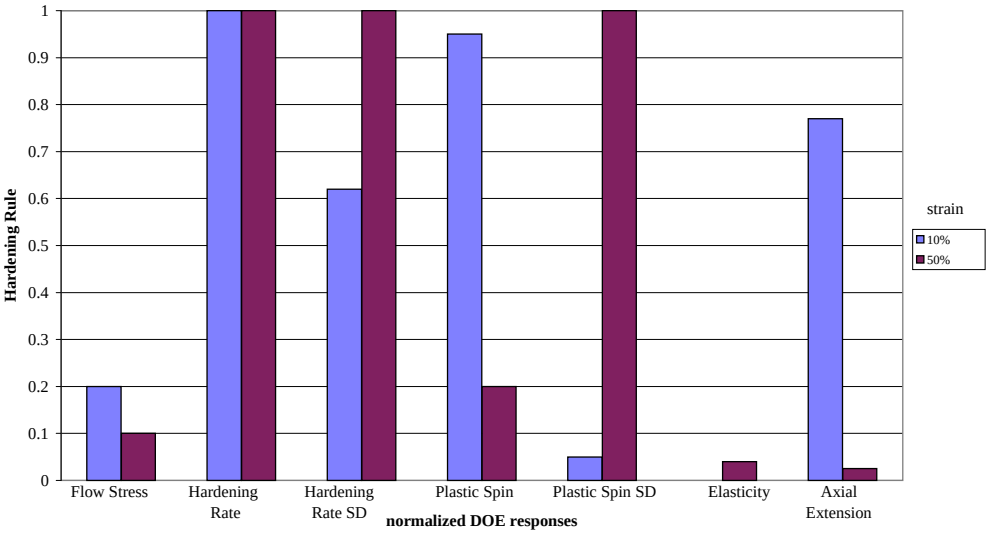

Figure 3. DOE influence of hardening rule on responses at 10% and 50% effective strain.

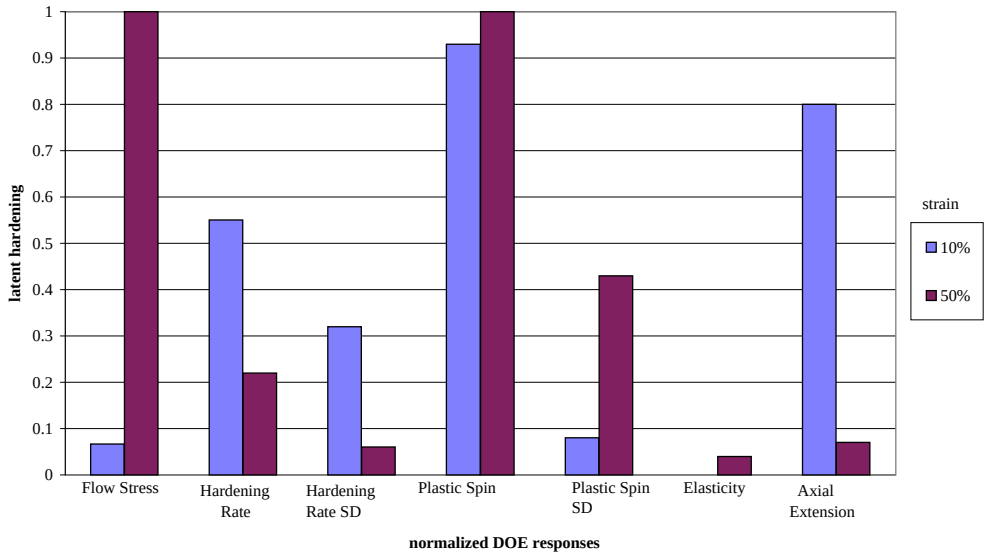

Figure 4. DOE influence of latent hardening on responses at 10% and 50% effective strain.

at 30% strain indicating its continued influence on the memory of the material up to 50% strain and even being the primary influence at that point. This was also observed in the planar 2D DOE analysis of Horstemeyer and McDowell (1997).

The hardening rule had a primary influence on the work-hardening rate, mean plastic spin, and axial extension at 10% strain as shown in figure 3. The influence of the hardening rule changed at 50% strain. It still had a primary influence on the work-hardening rate, but had a negligible influence on the mean plastic spin and axial extension. Otherwise at 50% strain, it

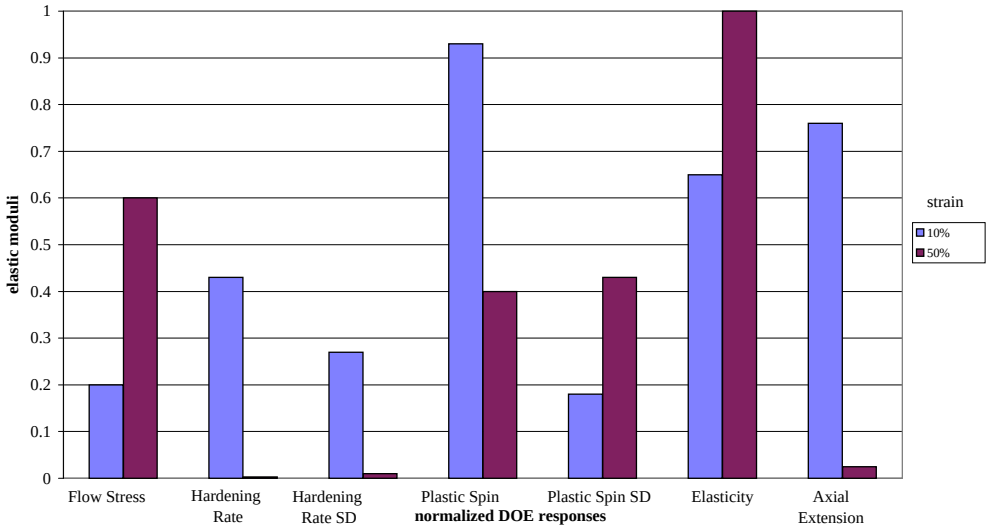

Figure 5. DOE influence of elastic moduli on responses at 10% and 50% effective strain.

had a primary influence on the spread of plastic spin and work-hardening rate. This is interesting because it indicates that the hardening rule affects texture which in turn influences these two macroscale quantities. The hardening rule had negligible effects on the polycrystalline elastic moduli and surprisingly on the flow stress.

Figure 4 shows that the latent hardening parameter had a primary influence on the plastic spin throughout deformation. It had an increasing influence from negligible to primary on the macroscale flow stress from 10% strain to 50% strain. By contrast, it had a decreasing influence from primary to negligible on the axial extension. On the hardening rate, elasticity, and spread of plastic spin the latent hardening influence was minimal to negligible.

The strongest influence on the polycrystalline elastic moduli was determined by whether the single-crystal elastic properties were anisotropic or isotropic, as shown in figure 5; this also had a primary influence on the plastic spin at 10% strain. It also had a secondary influence on the axial extension at 10% strain but decreased at 50% strain. Otherwise, it had minor-to-negligible effects on the other macroscale responses.

5.2. Macroscale response discussion

The macroscale effective flow stress was determined by taking the volume average of the in-plane shear component and then applying the von Mises criterion, i.e. $\sigma^{\text{eff}} = \sqrt{3}\sigma_{12}^{\text{ave}}$. Figure 6 shows that at 10% and 50% effective strain, the kinematic hardening had the primary influence. At 10% strain, every other parameter had a negligible influence. At 50% strain, although the kinematic hardening had a primary influence on the flow stress, it saturated at 30% strain. This indicates a memory effect still influencing the material. At 50% strain, we also see that latent hardening had a primary influence whereas at 10% strain, it was negligible. Elasticity and intergranular constraint increased in influence to a tertiary level as the applied deformation increased to 50% strain. The influence of the hardening rule was negligible.

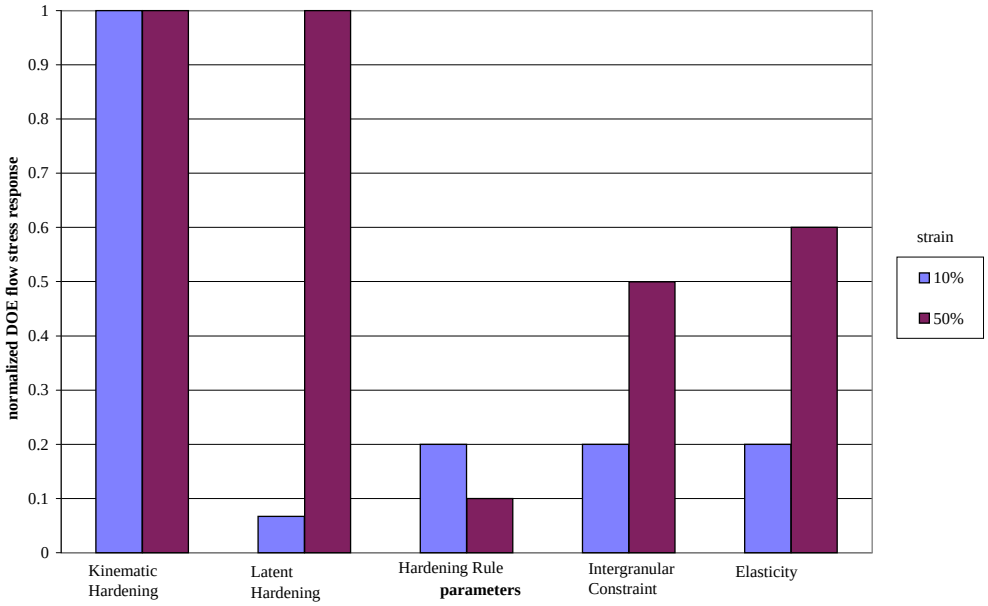

Figure 6. DOE polycrystalline flow stress results showing the relative influence of mesoscale parameters at 10% and 50% effective strain.

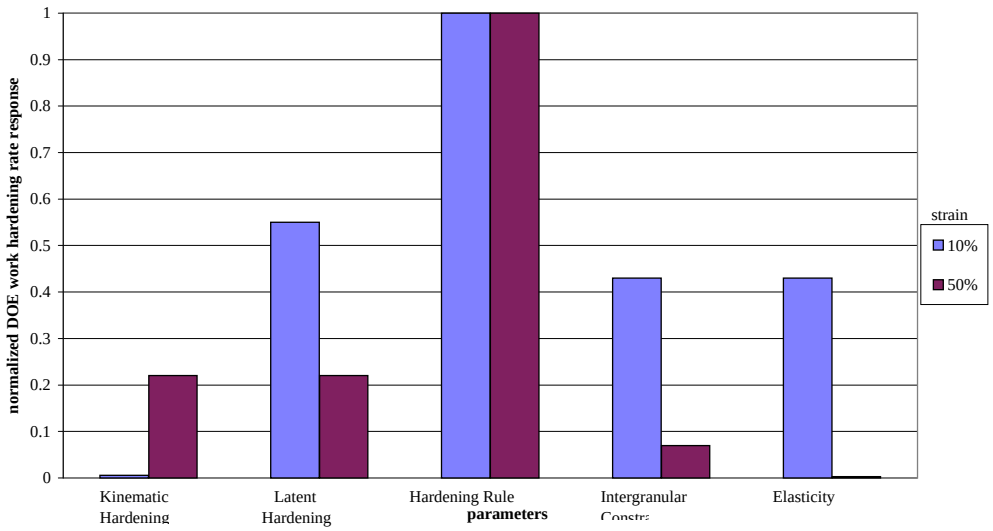

Figure 7. DOE polycrystalline mean work-hardening rate results showing the relative influence of mesoscale parameters at 10% and 50% effective strain.

Figures 7 and 8 show the responses of the mean and spread of the work-hardening rate as a function of the parameters at 10% and 50% strain. The polycrystalline work-hardening rate is defined by $\partial\sigma^{\text{eff}}/\partial\varepsilon^{\text{eff}}$. The hardening rule was the dominant influence on the mean and spread of the work-hardening rate. Interestingly, figures 7 and 8 show decreases in influence from latent hardening, intergranular constraint and elasticity from mainly a tertiary to a negligible influence as the applied deformation proceeded from 10% to 50% strain. The kinematic hardening had a negligible influence on the mean and spread of the work-hardening rate at

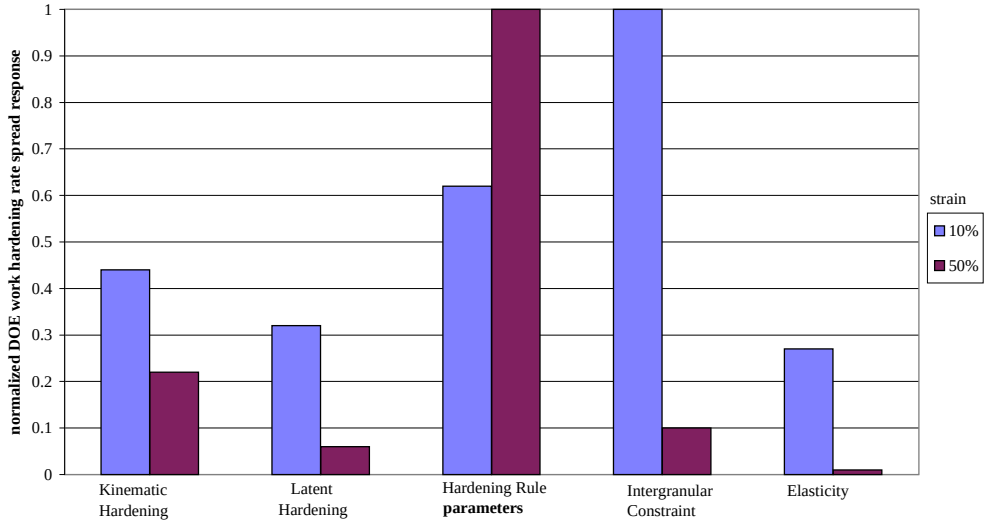

Figure 8. DOE polycrystalline spread of work-hardening rate results the relative influence of mesoscale parameters at 10% and 50% effective strain.

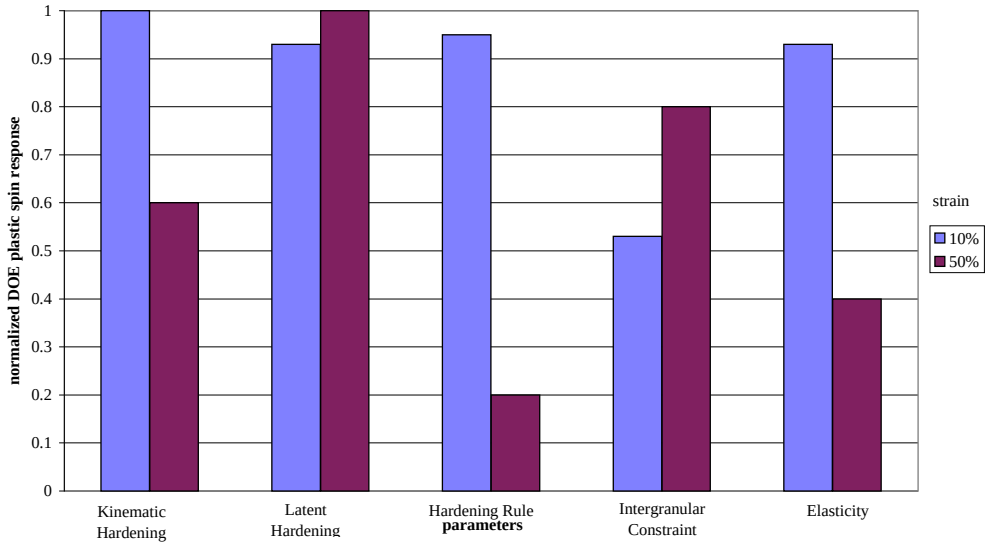

Figure 9. DOE polycrystalline mean plastic spin results showing the relative influence of mesoscale parameters at 10% and 50% effective strain.

50% strain, but had a tertiary influence on the spread of the work-hardening rate at 10% strain.

Figure 9 shows the responses of the mean plastic spin as a function of the parameters at 10% and 50% strain. The plastic spin of each grain was computed as follows,

$$\underline{W}^{\mathrm{p}} = \sum_{i=1}^{N} \dot{\gamma}_i \left(\underline{s}_i \otimes \underline{m}_i\right)_{\mathrm{anti}} . \tag{17}$$

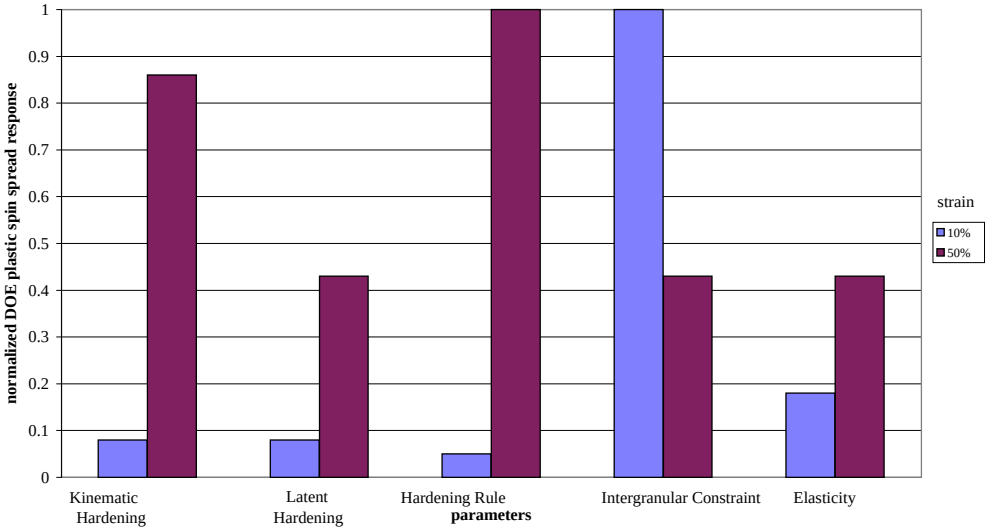

Figure 10. DOE polycrystalline spread of plastic spin results showing the relative influence of mesoscale parameters at 10% and 50% effective strain.

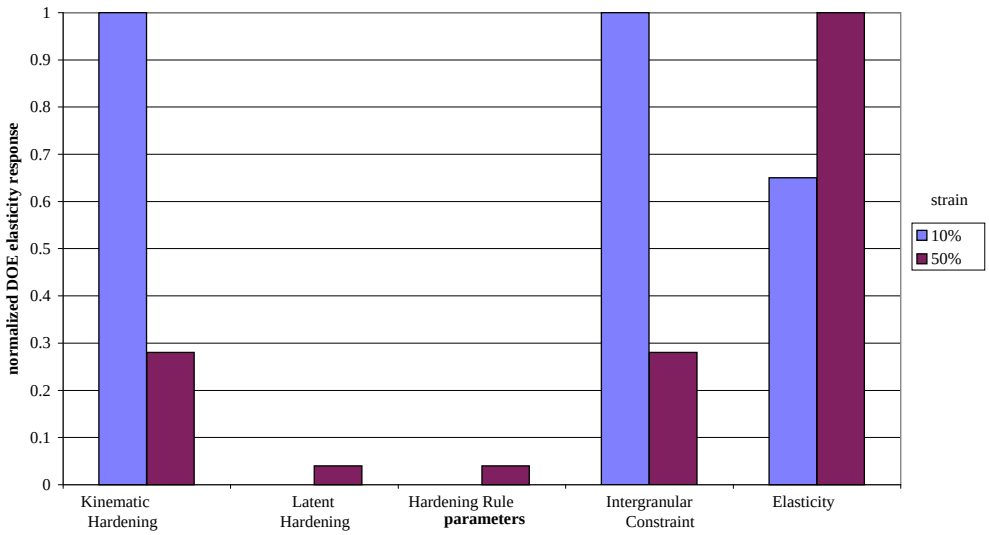

Figure 11. DOE polycrystalline elastic shear moduli results showing the relative influence of mesoscale parameters at 10% and 50% effective strain.

Since the macroscopic shear was imposed in the 1–2 direction, only W_{12}^{p} has been reported. The mean plastic spin is the numerical average of the individual grain values. Surprisingly, all the parameters had a relatively similar influence on the mean plastic spin as illustrated in figure 9. At 10% strain, the kinematic hardening, latent hardening, hardening rule, and elastic anisotropy all had a primary influence. The intergranular constraint had a tertiary influence at 10% strain. This indicates a tight coupling of the equations in determining the plastic spin. At 50% strain, the intergranular constraint and latent hardening had primary influences, as the influence of the kinematic hardening decreased to a secondary level. The influence of the elastic anisotropy decreased from a primary to a minor influence from 10% to 50% strain, and the hardening rule decreased from a primary to negligible influence from 10% to 50% strain.

Figure 10 shows that the primary influence on the spread of the distribution of plastic spin at 10% strain was the intergranular constraint with all the other factors being negligible. At 50% strain, the kinematic hardening and hardening rule surprisingly had primary influences. The intergranular constraint influence decreased to a tertiary level at 50% strain. Latent hardening and elasticity had negligible influences on the spread of plastic spin at 10% strain but increased to tertiary levels at 50% strain.

Figure 11 shows the responses of the polycrystalline elastic shear modulus as a function of the parameters at 10% and 50% strain. The polycrystalline elastic moduli were determined from the volume average over all the grains. As might be expected, the single crystal elastic moduli had a strong influence on the polycrystalline elastic moduli throughout the deformation, but more so at 50% strain because of the deformation-induced anisotropy. At 10% effective strain, the intergranular constraint and kinematic hardening played a primary role but lost influence to only a minor role at 50% strain. The latent hardening and hardening rule had negligible effects on the polycrystalline elastic shear modulus.

Figure 12 shows the responses of the axial extension as a function of the parameters at 10% and 50% strain. The polycrystalline axial extension developed during free-end shearing was determined by the volume average of the single-crystal axial extension. Note that all the parameters had a primary influence on the axial extension at 10% strain, but only the

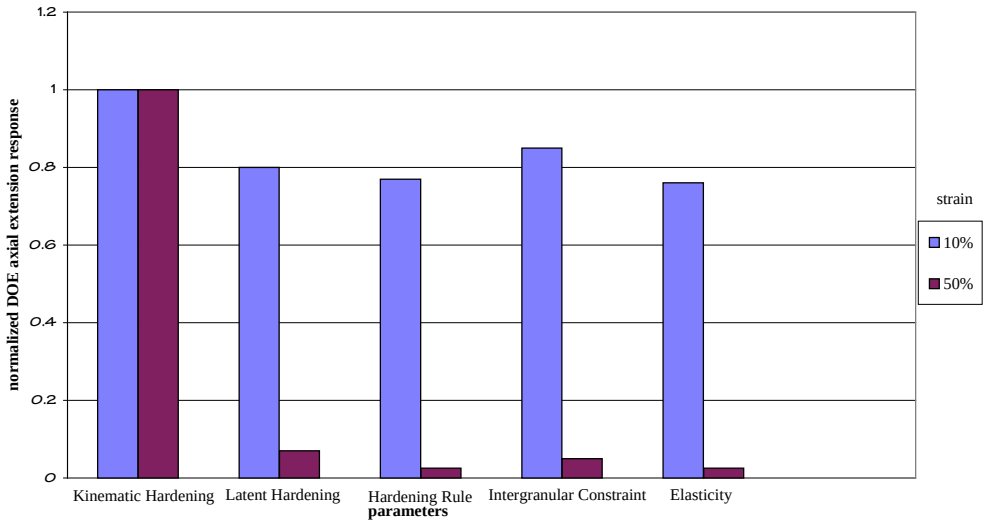

Figure 12. DOE polycrystalline axial extension results showing the relative influence of mesoscale parameters at 10% and 50% effective strain.

kinematic hardening retained a primary influence at 50% strain. At 50% strain the other parameters decreased such that they had a negligible influence.

The results in Figure 12 are similar to those for the plastic spin. Axial extension for free-end shear is a second-order effect and would be a result of the texture development like the plastic spin. This result is critical when considering the modelling of secondary responses, such as axial extension in free-end shear or axial stresses in fixed-end shear, with macroscale unified-creep-plasticity models. The axial stresses under fixed-end torsion and axial strains under free-end torsion have been attributed to texture effects (Harren *et al* 1989).

5.3. Comparison of planar double-slip with three-dimensional results

Horstemeyer and McDowell (1997) performed a similar DOE analysis in a planar double-slip context, and it is instructive to compare those results with these 3D results. Both studies showed that the intergranular constraint and kinematic hardening had the most influence on the macroscale parameters, but the 3D study showed a much stronger influence from latent hardening on the macroscale responses than the 2D study. This is somewhat surprising considering the differences in the two formulations. First, there is the obvious difference that the 2D double-slip formulation overconstrains the plasticity framework more than the 3D framework. Another difference was that the boundary condition in the 2D study was fixed-end shear while in the 3D study it was free-end shear. A self-consistent method was also used in the 2D study to relax the Taylor constraints but the finite-element method was used in the 3D study. Finally, the form of one of the hardening rules changed from the Chang–Asaro (Chang and Asaro 1981) hardening rule to the Armstrong–Frederick (Armstrong and Frederick 1966) hardening-recovery format. Even with these differences, the conclusions in the two studies were very similar with qualitative differences, only occurring in relation to the influence of latent hardening.

6. Summary

For a given material *and* for the given range of model features employed in this study, the DOE methodology has quantified the relative influence of different selected elements of standard polycrystal plasticity theory as a function of deformation level and path. Within this context, for the specific mesoscale constitutive relations selected for the study some key findings include the following.

- The introduction of kinematic hardening at the scale of individual grains (slip system) demonstrated a strong influence on the polycrystal flow stress, mean and spread of plastic spin, polycrystalline elastic shear modulus, and axial extension. The kinematic hardening had minor-to-negligible influences on the mean and spread of the work-hardening rate. In spite of the fact that kinematic hardening was introduced as a short range transient that saturated at 20% of the effective flow stress after 30% effective strain in monotonic deformation, it still had influence up to 50% strain.
- The intergranular constraint had a strong influence on the spread of the polycrystal work-hardening rate and plastic spin. At 10% strain, the intergranular constraint had a primary influence on the polycrystalline elastic moduli and on the axial extension.
- The choice of latent hardening had a greater influence in the 3D study than in the previous 2D study of Horstemeyer and McDowell (1997). The latent hardening played a primary role in the polycrystalline flow stress, mean plastic spin, and axial extension. It had a tertiary role in the mean and spread of the polycrystalline work-hardening rate and spread of plastic spin.

The range of constitutive model elements was not exhaustive in this study. For example, the results were indifferent to latent hardening for values of $q = 1$ or $q = 1.4$ for the Peirce–Asaro–Needleman formulation for both texture and stress–strain behaviour in shear and compression for OFHC Cu. Of course, the influence of this model in comparison with a radically different formulation of latent hardening (cf. Weng (1987)) might prove to be quite significant. Furthermore, a material such as aluminum, which has a lower hardening rate than copper and is more elastically isotropic, may generate different results.

In this study, only shear loading paths were considered. For reversed yielding or changes of the deformation path even more demanding, discriminatory requirements are placed on the elements of the constitutive models. The DOE methodology could be used for this type of loading path as well as a straightforward extension.

We emphasize that this DOE methodology provides the relative influence or the sensitivity of an aggregate performance index or response function to a range of mesoscale models for evolving structure and its effects. As such, the methodology may be useful as part of an overall strategy for optimization of constitutive laws that covers not only parameter estimation, but also the objective selection of the forms of the various elements such as hardening and constraint laws. Polycrystal plasticity is a good example of a nonlinear constitutive law with multiple sources and scales of nonlinearity. Generally, models that attempt to bridge vastly different length scales exhibit the same kind of amenability to the DOE approach. The results are also useful in guiding the disposition of effort to improve certain elements in order to achieve enhanced description. For example, if the precise form of the slip-system hardening rule does not significantly influence the macroscale average response function, then there is little impetus to refine it further, unless the form (e.g. dependent variables) is radically different. This sort of information is of an entirely different character to that offered by parameter optimization schemes, where the objective is to find a set of parameters that minimizes some error norm over the space of desired performance objectives for a *specific* constitutive model structure.

Acknowledgments

The work by M F Horstemeyer was performed under the U.S. Department of Energy contract number DE-AC04-94AL85000. D L McDowell and R McGinty are grateful for the support of the U.S. Army Research Office (Dr K Iyer, Program Manager) in conducting this and related research.

Appendix

The following table summarizes the elastic constants and plastic constants that were used for each of the parameters. Note that the plastic constants were determined by correlation with stress–strain curves from torsion experiments for OFHC Cu.

Table A1. Material constants for the eight calculations.

Constant	Units	1	2	3	4	5	6	7	8
C_1	GPa	168.4	210	168.4	210	210	168.4	210	168.4
C_2	GPa	121.4	100	121.4	100	100	121.4	100	121.4
C_3	GPa	75.5	55	75.5	55	55	75.5	55	75.5
M	–	10	10	10	10	10	10	10	10
h_0	MPa	–	–	72	72	133	133	–	–
Φ	–	–	–	11	11	21	21	–	–
γ_0	–	–	–	0.002	0.002	0.02	0.02	–	–
A	MPa	100	100	–	–	–	–	123	120
B	–	1.02	1.02	–	–	–	–	1.43	1.43
lhr	–	1.0	1.0	1.4	1.4	1.0	1.0	1.4	1.4
C_{sat}	MPa	18	18	18	18	18	18	18	18
C_{rate}	–	18.8	18.8	18.8	18.8	18.8	18.8	18.8	18.8

$\alpha_i = 0$ is an initial condition.

References

Armstrong P J and Frederick C O 1966 *CEGB Report* RD/B/N, p 731
Asaro R J 1983 *J. Appl. Mech.* **50** 921–34
Bassani J and Wu 1991 *Proc. R. Soc.* A **435** 21–41
Berveiller M and Zaoui A 1979 *J. Mech. Phys. Solids* **26** 325–44
Bishop J F W and Hill R 1951 *Phil. Mat.* **7**(42) 1298–307
Box G E, Hunter W G and Hunter J S 1978 *Statistics for Experimenters* (New York: Wiley *et al*)
Budiansky B and Wu T Y 1962 *Proc. 4th US National Congress of Applied Mechanics* p 1175
Chang Y W and Asaro R J 1981 *Acta Metall.* **29** 241–57
Cohen M 1976, *Mater. Sci. Engng*. **25** 3
Cuitino A M and Ortiz M 1992 *Modelling Simulation Mater. Sci. Eng.* **1** 225–63
Coleman B D and Gurtin M E 1967 *J. Chem. Phys.* **47** 597
Dawson P R 1987 *Int. J Solid Structures* **23**(7) 947–68
Dawson P R, Beaudoin A J and Mathur K K 1994 Numerical predictions of deformation processes and the behavior of real materials *Proc. 15th Riso Symposium on Materials Science (Riso National Laboratory, Roskilde, Denmark)* pp 33–44
Eshelby J 1957 *Proc. R. Soc.* A **241** 376–96
Fisher R A 1935a *Statistical Methods for Research Workers* (Oliver and Boyd)
——1935b *The Design of Experiments* (Oliver and Boyd)
France L K, Hartley C S and Reid C N 1967 *Metal Sci. J.* **1** 65–70
Franciosi, Berveiller M and Zaoui A. 1980 *Acta Metall*. **28** 273–83

Hansen N and Jensen J D 1991 Anisotropy and localization of plastic deformation *Proc. 3rd Symposium on Plasticity and Its Current Applications* ed J P Boehler and A S Khan, pp 131–4
Harren S, Lowe T C, Asaro R J and Needleman A 1989 *Phil. Trans. R. Soc.* A **238** 443–500
Havner K S 1982 *Mech. Mater*. **1** 97–111
Hill R 1965 *J. Mech. Phys. Solids* **13** 89–101
Hill R and Rice J R 1972 *J. Mech. Phys. Solids* **20** 401–13
Honneff W G and Mecking H 1978 *Texture of Materials* ed G Gottstein and K Lucke (Berlin: Springer) pp 265–75
Horstemeyer M F and McDowell D L 1997 Using statistical design of experiments for parameter study of crystal plasticity modeling features under different strain paths *Sandia National Laboratories Report* SAND96-8683
——1998 *Mechanics of Materials* at press
Hughes D A 1995 *Proc. 16th Riso International Symposium (Roskilde, Denmark)* ed N.Hansen *et al*
Hutchinson J W 1970 *Proc. R. Soc*. A **319** 247–72
——1976 *Proc. R. Soc*. A **348** 101–27
Jordan E H and Walker K P 1992 *J. Engng Mater. Tech*. **114** 19–26
Jordan E H, Shi S and Walker K P 1993 *Int. J. Plasticity* **9** 119–39
Kalidindi S R and Anand, L. 1991 *Advances in Finite Deformation Problems in Materials. Processing and Structures* **125** 3–14
Kalidindi S R, Bronkhurst C A and Anand L 1992 *J. Mech. Phys. Solids* **40**(3) 537–69
Kocks U F 1970 *Metall. Trans*. **1** 1121
——1976 *J. Engng Mater. Tech*. **98** 76–85
——1987 *Unified Constitutive Equations for Creep and Plasticity* ed A K Miller (New York: Elsevier) ch 1, pp 1–88
Kroner E 1961 *Acta Metall*. **9** 155
Lin T H 1957 *J. Mech. Phys. Solids* **5** 143
Lowe T C and Lipkin J 1990 Analysis of axial deformation response during reverse shear *Sandia National Laboratories Report* SAND90-8417
McDowell D L, Miller M P and Bammann D F 1991 Some additional considerations for coupling of material and geometric nonlinearities for polycrystalline metals *Proc. MECAMAT '91 (Fontainebleau, France)*
Miller M P 1993 *PhD Thesis* Georgia Institute of Technology
Mughrabi H 1978 *Mater. Sci. Engng* **33** 207–23
Nakada Y and Keh A S 1966 *Acta. Metall*. **14** 961–73
Nair V N 1992 *Technometrics* **34**(2) 127–61
Nair V N and Shoemaker A C 1990 *The Role of Experimentation in Quality Engineering: A Review of Taguchi's Contributions, Statistical Design and Analysis of Industrial Experiments* ed S Ghosh (New York: Marcel Dekker) pp 247–77
Nelder J A and Lee Y 1991, *Applied Stochastic Models and Data Analysis* **7** 107–20
Olson G B 1997 Advanced materials and processes **ASM News 7** 72–9
Phillips A and Das P K 1985 *Int. J. Plasticity* **1** 89
Phillips A and Gray G 1961 *J. Basic Engng Trans. ASME* **83** 275
Phillips A and Kasper R 1973 *J. Appl. Mech*. **40** 891
Peirce D, Asaro R J and Needleman A 1982 *Acta Metall*. **30** 1087–119
——1983 *Acta Metall*. **31** 1951–76
Rashid M M and Nemat Nasser S 1990 *Comput. Meth. Appl. Mech. Engng* **94** 201
Rashid M M, Gray G T III, Nemat Nasser S 1992 *Phil. Mag.* A **65**(3) 707–35
Rice J R 1971 *J. Mech. Phys. Solids* **9** 433–55
Taguchi G 1974 *Shaishin Igaku (The Newest Medicine*) **9** 806–13
——1986 *Introduction to Quality Engineering* (Tokyo: Asian Productivity Organization)
——G 1987 *System of Experimental Design* vols I and II (New York: UNIPUB)
Taylor G I 1938 *J. Inst. Metals* **62** 307
Taylor G I and Elam C F 1923 *Proc. R. Soc*. A **102** 643–67
Weng G J 1987 *Int. J. Plasticity*. **3** 315–39